water

MDPI

Article

Evaluating Curb Inlet Efficiency for Urban Drainage and Road Bioretention Facilities

Xiaoning Li [1,2], Xing Fang [1,3,*], Gang Chen [2], Yongwei Gong [3], Jianlong Wang [3] and Junqi Li [3]

1 Department of Civil Engineering, Auburn University, Auburn, AL 36849-5337, USA; xzl0055@auburn.edu
2 College of Hydrology and Water Resources, Hohai University, No. 1 Xikang Road, Nanjing 210098, China; gangchen@hhu.edu.cn
3 Key Laboratory of Urban Stormwater System and Water Environment, Ministry of Education, Beijing University of Civil Engineering and Architecture, Beijing 100044, China; gongyongwei@bucea.edu.cn (Y.G.); wjl_xt@163.com (J.W.); lijunqi@bucea.edu.cn (J.L.)
* Correspondence: xing.fang@auburn.edu; Tel.: +1-334-844-8778; Fax: +1-334-844-6290

Received: 4 April 2019; Accepted: 17 April 2019; Published: 23 April 2019

Abstract: An updated two-dimensional flow simulation program, FullSWOF-ZG, which fully (Full) solves shallow water (SW) equations for overland flow (OF) and includes submodules modeling infiltration by zones (Z) and flow interception by grate-inlet (G), was tested with 20 locally depressed curb inlets to validate the inlet efficiency (E_{ci}), and with 80 undepressed curb inlets to validate the inlet lengths (L_T) for 100% interception. Previous curb inlet equations were based on certain theoretical approximations and limited experimental data. In this study, 1000 road-curb inlet modeling cases from the combinations of 10 longitudinal slopes (S_0, 0.1–1%), 10 cross slopes (S_x, 1.5–6%), and 10 upstream inflows (Q_{in}, 6–24 L/s) were established and modeled to determine L_T. The second 1000 modeling cases with the same 10 S_0 and 10 S_x and 10 curb inlet lengths (L_{ci}, 0.15–1.5 m) were established to determine E_{ci}. The L_T and E_{ci} regression equations were developed as a function of input parameters (S_0, S_x, and Q_{in}) and L_{ci}/L_T with the multiple linear regression method, respectively. Newly developed regression equations were applied to 10,000 inlet design cases (10 S_0, 10 S_x, 10 Q_{in}, and 10 L_{ci} combinations) and comprehensively compared with three equations in previous studies. The 100% intercepted gutter flow (Q_{g100}) equations were derived, and over-prediction of Q_{g100} from previous methods was strongly correlated to smaller S_0. Newly developed equations gave more accurate estimations of L_T and E_{ci} over a wide range of input parameters. These equations can be applied to designing urban drainage and road bioretention facilities, since they were developed using a large number of simulation runs with diverse input parameters, but previous methods often overpredict the gutter flow of total interception when the longitudinal slope S_0 is small.

Keywords: curb inlet; overland flow; two-dimensional simulation; bioretention; intercepted flow; inlet efficiency

1. Introduction

The urban drainage system is designed and built to effectively convey the rainfall runoff out of the urban area to prevent inundation and local flooding [1], which can cause property damage and affect traffic and human safety. Curb inlets effectively intercept surface runoff into underground drainage pipes or bioretention facilities. As an important and typical practice, road bioretention facilities, which combine green/gray infrastructures to facilitate road runoff control through infiltration and storage, remove certain contaminants and sediments, and decrease roads' local flood inundation risk, are widely used in the pilot Sponge City construction in China [2] and all over the world. Li et al. [3] found that the curb inlet could be the bottleneck of road bioretention facilities that impedes the runoff

generated from the road flowing into the bioretention to infiltrate, detain (pond), and improve the stormwater quality. Tu and Traver [4] found that the perforated distribution pipe could be an uncertain factor on road bioretention performance. Stoolmiller et al. [5] surveyed curb inlets for road bioretention facilities in Philadelphia, and the curb inlet opening ranged from 0.15 m (6 inches) to 1.52 m (5 ft). Some of these inlets seem to have been designed based on the landscape and from a safety perspective, instead of hydraulic performance considering inlet interception efficiency.

There are three types of curb inlets commonly used along urban streets. The undepressed curb inlet has one cross slope for the road, gutter, and curb inlet. The continuously depressed curb inlet is placed in the gutter of a street with a steeper cross slope than the road cross slope [6]. The locally depressed curb inlet has adjacent depressions in the gutter before and/or after the inlet for effective flow interception—for example, type C and type D curb inlets, designed and constructed by the Texas Department of Transportation (TxDOT) [7], have a 5 to 15 ft locally depressed curb opening, and 5 ft transition sections at the upstream and downstream of the opening (Figure 1). The upstream transition section changes elevation gradually from the undepressed section into fully depressed inlet section over the 1.52 m (5 ft) length, and the downstream transition section gradually decreases the local depression (Figure 1).

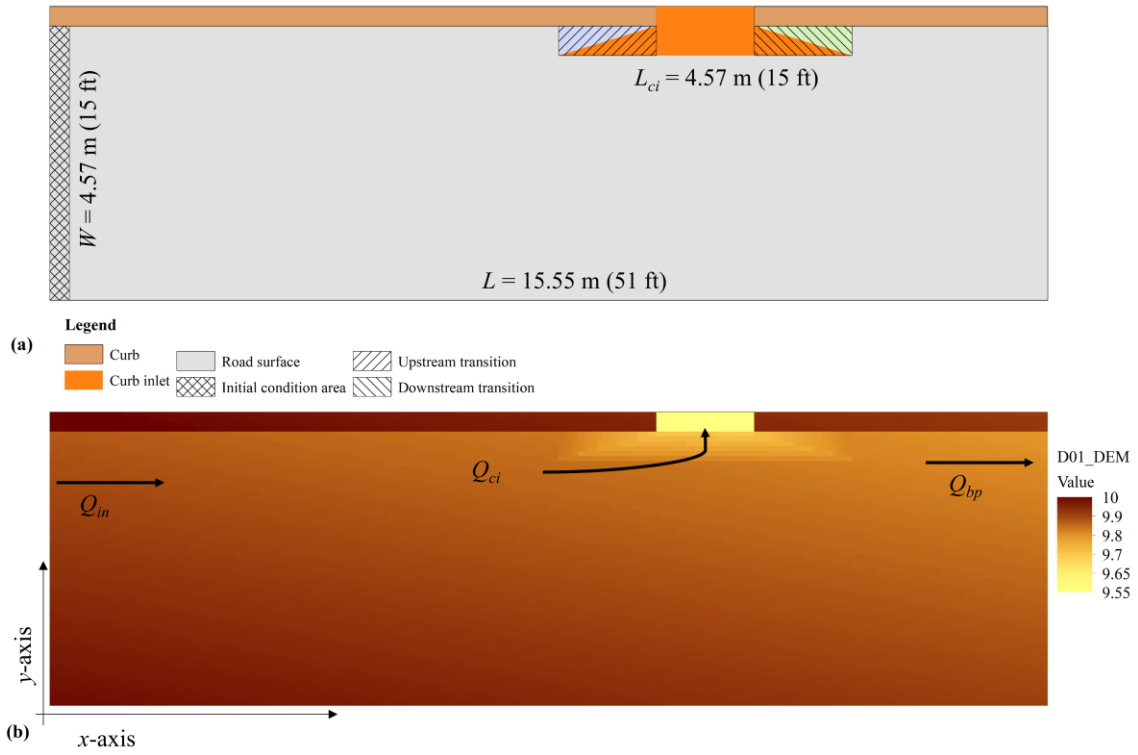

Figure 1. (**a**) Layout of the Type D curb inlet evaluation experiment, and (**b**) digital elevation model (DEM) of case D01 with S_0 = 0.004 and S_x = 0.0208.

The hydraulic performance of curb inlets for roadway drainage has been studied for more than 60 years, which was reviewed and summarized by Izzard [8], Li [9], and presently systematically documented in the Hydraulic Engineering Circular No. 22 (HEC-22) by Brown et al. [10]. In 1979, the Federal Highway Administration [11] first published a technical guide for the design of urban highway drainage, and then updated it in 1984 into a HEC-12 entitled "Drainage of Highway Pavement" [12]. HEC-12 summarizes a semi-theoretical method developed for estimating street hydraulic capacities and procedures for sizing street inlets. The most recent HEC-22 [10] was published and widely used in the USA, and refined the design procedures stated in HEC-12.

Izzard [8] developed equations to calculate the normal depth of gutter flow and the curb opening length (L_T) (Equation (1)) required to intercept 100% of the gutter flow. Izzard [8] assumed that the

transverse velocity of the approach flow to an inlet was zero and that the hydraulic head decreased linearly along the curb inlet. Izzard (1950) applied the usual form of Manning's equation in a local sense, and calculated the total gutter flow via integrating dQ at each section and across the flow area with a uniform cross slope. Izzard (1950) compared his theoretical equation to unpublished data from experiments with less than 100% efficiency on undepressed curb inlets conducted at the University of Illinois, and determined the coefficient value in Equation (1):

$$L_T = 1.477 Q_{in}^{7/16} S_0^{9/32} / (nS_x)^{9/16} \quad (1)$$

where L_T is in m, Q_{in} is the upstream inflow (m^3/s), S_0 is the longitudinal slope of the road or gutter, and S_x is the cross slope (Figure 1), and n is Manning's roughness coefficient. Izzard [8] developed Equation (2) to calculate the efficiency (E_{ci}) of a curb inlet, which is the ratio of flow intercepted by the curb inlet (Q_{ci}) and the gutter flow Q_{in} of undepressed curb inlet with the opening length of L_{ci} (m).

$$E_{ci} = \frac{Q_{ci}}{Q_{in}} = 1 - \left(1 - \frac{L_{ci}}{L_T}\right)^{5/2} \quad (2)$$

For the undepressed curb inlet, Equations (3) and (4) were adapted by HEC-22 [10] to determine L_T and E_{ci}.

$$L_T = 0.817 Q_{in}^{0.42} S_0^{0.3} / (nS_x)^{0.6} \quad (3)$$

$$E_{ci} = 1 - [1 - (L_{ci}/L_T)]^{1.8} \quad (4)$$

Muhammad [13] summarized previous curb inlet efficiency evaluation studies and proposed Equation (5) to calculate L_T and Equation (6) to calculate E_{ci}.

$$L_T = 0.101 Q_{in}^{0.47} S_0^{0.26} / \left(n^{0.95} S_x^{0.75}\right) \quad (5)$$

$$E_{ci} = 1 - [1 - (L_{ci}/L_T)]^{\alpha} \quad (6)$$

where α is not a constant, but calculated with an equation $\alpha = \frac{0.42}{S_x^{0.42}}$. When S_x ranges from 1.5% to 6%, α changes from 2.45 to 1.37.

Guo and MacKenzie [14] stated that the HEC-22 procedure overestimates the capacity of a curb-opening inlet when water depth is shallow, and then becomes underestimating when water depth exceeds 7 inches for 3 ft curb inlet in the sump. To determine inlet efficiency and performance, the reduced-scale physical models were used and based on Froude number scaling—that is, a 3:4 scale model for Hammonds and Holley's study [7], 1:4 for Uyumaz's research [15], and 1:3 for Guo and Mackenzie's tests [14]; only Schalla et al. [16] conducted full-scale experiments for the curb inlet. The scaling effect has recently been discussed as a possible reason for significant discrepancies in interception efficiency between field measurements and predictions of the regression equations based on scaled laboratory experiments [17,18].

Much more attention and focus should be paid on studying the interception efficiency of a curb inlet and its design because it is an important component for urban drainage and road bioretention facilities. Most of the currently used curb inlet E_{ci} equations were based on simple theoretical derivation with assumptions and revised coefficients or exponents determined using experimental data. In this study, the two-dimensional numerical models were first developed to represent 20 full-scale laboratory experiments of locally depressed curb inlets conducted by Hammonds and Holley [7] and 80 experiments for undepressed curb inlets by Wesley [19] using high-resolution digital elevation models (DEMs) for the model validation study. The overland flow on the road with curb inlets and upstream inflow was simulated using the FullSWOF-ZG program [3], which was updated/reconfigured from an open-source two-dimensional overland flow program, FullSWOF_2D [20]. One thousand modeling cases of a road with an undepressed curb inlet with 10 S_0, 10 S_x, and 10 Q_{in} were then established and modeled to develop L_T for the 100% interception of gutter flow, and then a regression

equation of L_T as a function of input parameters was developed by the multiple linear regression method. The second 1000 modeling cases of the road with 10 S_0, 10 S_x, and 10 curb inlet lengths L_{ci} were established and simulated to determine E_{ci} of different L_{ci}, and a regression equation of E_{ci} as a function of L_{ci}/L_T was also developed. The simulation results of L_T and E_{ci} were discussed and comprehensively compared with calculated/predicted results from HEC-22 [10], Izzard [8], and Muhamad [13]. In this study, the height of the opening of the curb inlets was not directly considered when a two-dimensional model was used. Only under severe flood situations was the height of the opening found to play a role on flow interception and inlet efficiency.

2. Materials and Methods

Fang et al. [21] used a three-dimensional computational fluid dynamics (CFD) software, Flow-3D, to develop the numerical models simulating unsteady, free-surface, shallow flow through Type C and Type D [7] curb-opening inlets. They demonstrated that an advanced CFD model could be used as a virtual laboratory to evaluate the performance of curb inlets with different geometry and inflow conditions. In this study, the two-dimensional open source FullSWOF_2D (version 1.07, Dieudonné Laboratory J.A., Polytech Nice Sophia, Nice, France) [20] program was updated to simulate the complex flow through an inlet to determine the inlet-opening length L_T of 100% (total) interception, and the efficiency E_{ci} of an undepressed curb inlet.

The FullSWOF_2D program fully solves shallow-water equations (SWEs) [20], depth-integrating the Navier–Stokes equations [22] on a structured mesh (square cells) in two-dimensional domains using the finite volume method [23], and is programmed using C++ to fully describe the rainfall-runoff and flow distribution progress on the surface [24]. As a Saint-Venant system [22], the SWEs model is widely used to simulate the incompressible Navier–Stokes flow occurring in rivers, channels, ocean, and land surfaces [25]. It is derived with two assumptions: the water depth is small with respect to the horizontal (x, y) dimensions, and the pressure of the fluid is hydrostatic ($\partial p/\partial z = -g$), which means the pressure field could be calculated with simple integration along the vertical (z) direction [26]. A well-balanced numerical scheme was adapted to guarantee the positivity of water height and the preservation of steady states for specific hydrological features, such as during wet–dry transitions and tiny water depth [27]. Different boundary conditions, friction laws, and numerical schemes were developed, which make the program a very powerful overland flow simulation software [20].

The FullSWOF_2D program, which applies the uniform rainfall and infiltration parameters to the whole simulation domain, was revised by Li et al. [3] to include 2D plane zones (Z) with different rainfall and infiltration parameters and a 2D-1D grate-inlet (G) drainage module. Therefore, the updated FullSWOF-ZG program can simulate impervious and pervious surfaces (different infiltration parameters/capabilities in different zones) in the road bioretention domain simultaneously under rainfall events. The 2D-1D grate-inlet drainage submodule enables the program to simulate the 2D overland runoff flowing into a grate inlet, and then to a 1D underground drainage pipe using the weir equation [28]. In Li's study [3], the FullSWOF-ZG was used to evaluate the performance of a road bioretention facility and explore/understand key parameters of continuous road bioretention design. It was found that the curb inlet becomes the bottleneck of the road bioretention strip system that could impede the runoff flowing into the bioretention strip for detention and infiltration to improve the stormwater quality [3].

2.1. FullSWOF-ZG Validation Cases

For the reduced-scale and full-scale laboratory experiments, the curb inlet efficiency was calculated with flow intercepted by the curb inlet divided by the total upstream inflow, which did not consider the rainfall-runoff generation and concentration process. It was not meant to understand the performance of the curb inlet under a rainfall event, but to provide the information for engineering design of the curb inlet as a function of upstream inflow. Inflows with different magnitudes and spreads for curb inlets include runoff from upstream and surrounding lands and runoff produced from the roadway.

Therefore, these experimental studies are valuable, and numerical model studies under the same experimental conditions were used to validate the FullSWOF-ZG model to see how well the model can predict the curb inlet efficiency. Twenty locally depressed curb inlet cases, which were tested in a laboratory by Hammonds and Holley [7], were used to validate FullSWOF-ZG for curb inlet efficiency simulation. Eighty undepressed curb inlet cases, which were tested in a laboratory by Wesley [19], were used to validate FullSWOF-ZG for curb inlet lengths of 100% interception.

2.1.1. Modeling Cases to Validate Curb Inlet Efficiency

The FullSWOF-ZG program was previously tested and verified for overland flow on pervious surfaces [3,29]. In a previous study [3], the FullSWOF-ZG program was tested with 20 type C curb inlet cases. The coefficient of determination (R^2) of the linear relationship between the simulated and observed curb inlet interception efficiencies was 0.94 for type C curb inlet test cases. The differences between the simulated and observed interception efficiencies (ΔE) ranged from −3.2% to 13.2%, with an average ± standard deviation of 3.5 ± 3.5%. In this study, FullSWOF-ZG was first tested using 20 locally depressed curb inlets (type D, Figure 1), which was tested in laboratory experiments by Hammonds and Holley [7]. For type D curb inlet experiments, the length and width of the simulation domain were 15.55 m (51 ft, x-direction) and 4.57 m (15 ft, y-direction), respectively. The total opening lengths of different curb inlets were either 4.57 m (15 ft) or 7.62 m (25 ft), which included a 1.52 m (5 ft) or 4.57 m (15 ft) inlet opening and 1.52 m (5 ft) upstream and downstream transition sections (Figure 1). The total width of the curb inlet depression was 0.457 m (1.5 ft), and the depressed depth was 0.10 m (0.33 ft) and 0.076 m (0.25 ft) at a depression width of 0.368 m (1.2 ft) for type C and type D curb inlets, respectively.

The simulation domain was represented by a detailed and high-resolution DEM (Figure 1b) with a cell size equal to 0.076 m (0.25 ft). The elevation of every computation cell was calculated using a user-developed MATLAB r2017a (MathWorks, Natick, MA, United States) [30] code with consideration of the road's longitudinal slope, cross slope, locally depressed cross slope of the curb inlet, and the slopes of the inlet's upstream and downstream transition parts. The longitudinal (x-direction) and cross (y-direction) slopes for the simulation domain are from left to right and bottom to top, respectively (Figure 1). Manning's law in FullSWOF-ZG was used in the simulation, and the roughness coefficient determined for the laboratory roadway was 0.018 [7].

The imposed discharge condition in FullSWOF-ZG was chosen as the left or upstream boundary condition of the domain. The imposed discharge for the boundary cells within the spread (T) was approximately assumed as the total inflow rate (Q_{in}) divided by the number of the cells within the spread and set to be equal to 0 for other boundary cells outside of the spread. The top and right (downstream) boundary of the simulation domain was set as a Neumann condition that allows the flow to get out of the simulation domain. At the top of the simulation domain, those cells on the curb had higher elevations to prevent the outflow. The bottom boundary of the simulation domain (Figure 1b) had the highest elevation along the y-direction, and was set as a wall boundary condition to guarantee that the flow would not pass through the bottom boundary.

2.1.2. Modeling Cases to Simulate/Validate Curb Inlet Length of 100% Interception

Wesley [19] conducted a series of full-scale experiments to determine the 100% intercepted curb inlet lengths with different longitudinal and cross slopes for undepressed curb inlets. The experiment facility had a triangular cross-section with the curb side being nearly vertical, and placed on a continuous grade with no local depression on the channel bottom. The length of the curb opening was sufficient to allow for interception of all the flow from the upstream road. The experiment facility was 50 ft (15.24 m) in overall length and 6 ft (1.83 m) in width. At 32 ft (9.75 m) from the upstream end, the curb inlet opening began. This upstream length (32 ft) is sufficient for the development of a uniform flow condition. The 100% intercepted curb inlet length was then experimentally determined using the observed distribution of water depth along the curb [19].

The simulation domain was represented by detailed and high-resolution DEM with a smaller cell size equal to 0.05 ft (0.015 m), similar to Figure 1 without local depressions. The Manning's value was 0.01, which is the same as the experiment facility. For eighty experimental cases, S_0 ranged from 0.005 to 0.05, S_x ranged from 0.01 to 0.08, and upstream inflow Q_{in} ranged from 0.18 L/s to 84.38 L/s, which were simulated to determine the 100% interception curb inlet lengths.

2.2. Modeling Cases to Evaluate 100% Interception Length and Curb Inlet Efficiency

After the FullSWOF-ZG model was validated to be able to accurately simulate flow over the curb inlet, 1000 modeling cases were selected and modeled to determine the curb inlet length L_T of 100% interception under different S_0, S_x, and Q_{in}. The length and width of the simulation domain for these 1000 modeling cases were 12 m (x-direction) including the 10 m road surface before the inlet and 6.7 m (y-direction, Figure 1) including a 3 m wide car lane stripe, 1.5 m wide bike lane strip, 2.1 m parking stripe (1.5 m + 0.6 m gutter), and 0.1 m curb width. The cell size of DEMs for all 1000 cases was 0.025 m, determined by a sensitivity analysis.

Commonly used S_0 and S_x values in stormwater drainage design were chosen from the HEC-22 [10] for 1000 modeling cases, which are the combinations of 10 longitudinal slopes S_0, 10 cross slopes S_x, and 10 upstream inflows Q_{in} (Table 1). Ten S_0 slopes ranged from 0.1 to 1% with an increase interval of 0.1% and ten S_x from 1.5 to 6% with an increase interval of 0.5%, respectively. Ten upstream inflows which ranged from 6 to 24 L/s with an interval increase of 2 L/s were adapted for the simulation. The case number was named using the sequence number (1 to 10) of the parameter's choice of S_0, S_x, and Q_{in}; for example, the modeling case O1X1Q1 (Table 1) meant the road had S_0 = 0.001 (0.1%) and S_x = 0.015 (1.5%) with Q_{in} = 6 L/s for upstream inflow. The curb length was set to be large enough to intercept 100% inflow for all 1000 modeling cases.

Table 1. Sequence numbers and corresponding geometry and inflow parameters of modeling cases used for FullSWOF-ZG simulations, and the results for the 20 sample cases.

Sequence No.	S_0 (%)	S_x (%)	Modeling Case Index [1]	Q_{in} (L/s)	L_T (m)	Modeling Case Index [2]	L_{ci} (L_{ci}/L_T) (m) [3]	E_{ci} (%)
1	0.1	1.5	O1X1Q1	6	3.11	O1X1L1	0.15 (0.05)	15.3
2	0.2	2.0	O2X2Q2	8	3.46	O2X2L2	0.30 (0.09)	26.4
3	0.3	2.5	O3X3Q3	10	3.79	O3X3L3	0.45 (0.12)	34.9
4	0.4	3.0	O4X4Q4	12	4.06	O4X4L4	0.60 (0.15)	41.8
5	0.5	3.5	O5X5Q5	14	4.31	O5X5L5	0.75 (0.17)	48.0
6	0.6	4.0	O6X6Q6	16	4.56	O6X6L6	0.90 (0.20)	53.8
7	0.7	4.5	O7X7Q7	18	4.76	O7X7L7	1.05 (0.22)	59.3
8	0.8	5.0	O8X8Q8	20	4.99	O8X8L8	1.20 (0.24)	64.8
9	0.9	5.5	O9X9Q9	22	5.16	O9X9L9	1.35 (0.26)	70.2
10	1.0	6.0	O10X10Q10	24	5.34	O10X10L10	1.50 (0.28)	75.7

Note: [1]—modeling case for determining curb inlet length L_T of 100% interception, [2]—modeling cases for determining inlet efficiency E_{ci} of different length L_{ci} when Q_{in} = 10 L/s, and [3]—L_{ci} in m is given outside of brackets and the ratio L_{ci}/L_T is given inside of brackets (dimensionless).

To evaluate the curb inlet efficiency E_{ci} at different inlet lengths, the second 1000 modeling cases were selected using 10 choices of L_{ci} and the same 10 choices for S_0 and S_x, which were used for the 100 modeling cases to determine L_T. Ten curb inlet lengths L_{ci} ranged from 0.15–1.5 m (6–60 inches) with an increase of 0.15 m (6 inches), which was adapted based on the curb inlet survey conducted by Stoolmiller et al. [5]. The imposed upstream inflow Q_{in} was chosen as 10 L/s for the left boundary condition of the domain for the second 1000 modeling cases, and a part of the inflow was intercepted by the curb inlet—that is, Q_{ci} in Figure 1—and the remainder of the inflow was discharged downstream along the road (Q_{bp}), where the inlet length L_{ci} was less than L_T for 100% interception.

All cells' elevations were calculated using a MATLAB program when the bottom-left corner reference cell's elevation (the highest in the domain) was assumed to be 10 m (Figure 1b). The road surface ground elevations, therefore, varied with longitudinal and cross slopes set for each modeling case (Figure 1b). All cells for the 0.1 m curb were set 0.2 m higher than the road surface cells. The cell's

elevations inside the curb inlet cells were calculated using the same cross slope of the road surface, which helps and allows the runoff to flow out the road surface. The total simulation duration was 120 s (1.5 min) for reaching an equilibrium condition to determine E_{ci}.

3. Results and Discussion

3.1. FullSWOF-ZG Validation Results of Curb Inlet Efficiency

For the 20 modeling cases conducted for the type D inlet, geometry (S_0, S_x, and L_{ci}) and flow (Q_{in} and T) parameters have been listed in Table 2, and the same for the experimental conditions [7,21], which cover five longitudinal slopes (0.004–0.06), two cross slopes (0.0208 and 0.0407), 17 spreads (1.05–4.27 m), and 19 upstream inflows (0.0285–0.2597 m^3/s). Table 2 shows that simulated intercepted flows (Q_{cis}) and inlet efficiencies (E_{cis}) matched well with the observed results (Q_{cio} and E_{cio}) from the laboratory experiments conducted by Hammonds and Holley [7]. The coefficient of determination (R^2) of the linear relationship between simulated and observed E_{ci} is 0.99. The differences (ΔE in Table 2) of simulated and observed E_{ci} ranged from −2.28% to 4.21% with average ± standard deviation as 1.10% ± 1.67%. The percent differences (PD_E) of simulated and observed E_{ci} ranged from −3.15% to 5.17% with average ± standard deviation as 1.57% ± 2.29%. Therefore, the FullSWOF-ZG program can accurately simulate the overland flow through the road surface, gutter, local depressions (transition), and the flow interception over Type D curb inlets, and predict the curb inlet interception efficiency well.

Table 2. Geometry and inflow parameters and simulation results of 20 Type D locally depressed curb inlet modeling cases.

Case No.	S_0 (%)	S_x (%)	L_{ci} (m)	T (m)	Q_{in} (m^3/s)	Q_{cio} (m^3/s)	E_{cio} (%)	Q_{cis} (m^3/s)	E_{cis} (%)	ΔE (%)	PD_E (%)
D01	0.4	2.08 [1]	1.52	3.05	0.0427	0.0419	98.1	0.0425	99.4	1.3	1.3
D02	0.4	2.08	1.52	4.27	0.1113	0.0768	69.0	0.0803	72.2	3.2	4.5
D03	1.0	2.08	1.52	2.32	0.0326	0.0318	97.5	0.0324	99.3	1.8	1.8
D04	1.0	2.08	1.52	4.27	0.2424	0.1004	41.4	0.1037	42.8	1.4	3.2
D05	4.0	2.08	1.52	3.07	0.1361	0.0640	47.0	0.0649	47.7	0.6	1.4
D06	6.0	2.08	1.52	4.27	0.2279	0.0735	32.3	0.0771	33.8	1.6	4.8
D07	0.4	4.17 [2]	1.52	2.4	0.0702	0.0688	98.0	0.0687	97.9	−0.1	−0.1
D08	0.4	4.17	1.52	3.33	0.1677	0.1197	71.4	0.1160	69.2	−2.2	−3.2
D09	1.0	4.17	1.52	1.99	0.0634	0.0612	96.5	0.0621	98.0	1.5	1.5
D10	1.0	4.17	1.52	2.88	0.1659	0.1092	65.8	0.1083	65.3	−0.5	−0.8
D11	2.0	4.17	1.52	1.63	0.0523	0.0511	97.7	0.0513	98.2	0.5	0.5
D12	2.0	4.17	1.52	2.64	0.1659	0.0967	58.3	0.0966	58.2	−0.1	−0.1
D13	4.0	4.17	1.52	1.25	0.0370	0.0357	96.5	0.0361	97.4	1.0	1.0
D14	6.0	4.17	1.52	1.05	0.0285	0.0279	97.9	0.0273	95.6	−2.3	−2.4
D15	4.0	2.08	4.57	4.03	0.1599	0.1137	71.1	0.1197	74.9	3.8	5.2
D16	6.0	2.08	4.57	4.27	0.1802	0.1156	64.2	0.1195	66.3	2.1	3.3
D17	0.4	4.17	4.57	3.53	0.1887	0.1874	99.3	0.1885	99.9	0.6	0.6
D18	1.0	4.17	4.57	3.41	0.2597	0.2270	87.4	0.2379	91.6	4.2	4.7
D19	2.0	4.17	4.57	2.92	0.2309	0.2024	87.7	0.2071	89.7	2.0	2.3
D20	6.0	4.17	4.57	1.91	0.1451	0.1295	89.2	0.1320	91.0	1.7	1.9

Note: [1]—cross slope 2.08% is 1 vertical versus 48 horizontal (1:48), and [2]—cross slope 4.17% is 1:24. S_0 (%) is road longitudinal slope, S_x (%) is road cross slope, L_{ci} (m) is type D curb inlet depressed part length, T (m) is upstream flow spread width, Q_{in} (m^3/s) is upstream inflow rate, Q_{cio} (m^3/s) is observed curb inlet intercepted flow rate, E_{cio} (%) is observed curb inlet intercepted efficiency, Q_{cis} (m^3/s) is simulated curb inlet intercepted flow rate, E_{cis} (%) is simulated curb inlet intercepted efficiency, ΔE (%) is difference of simulated intercepted efficiency = $E_{cis} - E_{cio}$, PD_E (%) is percent difference of simulated intercepted efficiency = $(E_{cis} - E_{cio})/[(E_{cis} + E_{cio})/2] \times 100\%$.

The simulation results in Table 2 were first developed using the cell size of 0.076 m (0.25 ft) for square computational grids. Three other cell sizes (0.05 m, 0.025 m, and 0.01 m) were then used for 10 modeling cases of undepressed inlets (O10X10L1–O10X10L10 in Table 1) to conduct the cell size sensitivity analysis on a ThinkStation Desktop computer with central processing unit (CPU) type of Intel(R) Xeon (R) E3-1241 v3 3.5 GHz. For these three cell sizes, the total number of cells in the simulation domain (12 × 6.7 m) was 32,160, 128,640, and 804,000, respectively. For the 10 cases with a cell size of 0.05 m, the simulation time ranged from 0.15 h to 0.17 h with an average simulation time

equal to 0.15 h. For the 10 cases with a cell size of 0.025 m, the simulation time ranged from 1.23 h to 1.43 h with an average simulation time equal to 1.27 h. For the 10 cases with a cell size of 0.01 m, the simulation time ranged from 26.3 h to 26.4 h. The cell size of 0.025 m (~1 inch) was chosen as the simulation cell size for simulations of all other modeling cases in this study based on the balance of the model accuracy in predicting Q_{ci} and E_{ci} and the simulation time for the 10 test cases above.

3.2. Validation Results of 100% Intercepted Curb Inlet Length

The simulated water surface profile along the curb inlet was outputted and used by a MATLAB code to determine the 100% interception curb inlet length L_T. Figure 2a shows six examples of the simulated water surface profile along the curb for six selected L_T validation cases (WS11, 23, 34, 47, 56, and 73) out of 80 experiment tests (WS1–WS80) conducted by Wesley [19]. Because the curb inlet opening starts at 9.75 m, the water depth drops sharply at the first 0.2 m of the curb inlet opening and then decreases slowly and linearly along the curb inlet. Finally, the water depth becomes very small (a thin layer of water) across the remaining inlet length. These water surface profiles along the curb inlet show similar variations with distance as reported by other research studies, such as Schalla [16], Hodges et al. [31], and Muhammad [13], but are significantly different from the linear decrease assumption made and used by Izzard [8] to develop the L_T equation.

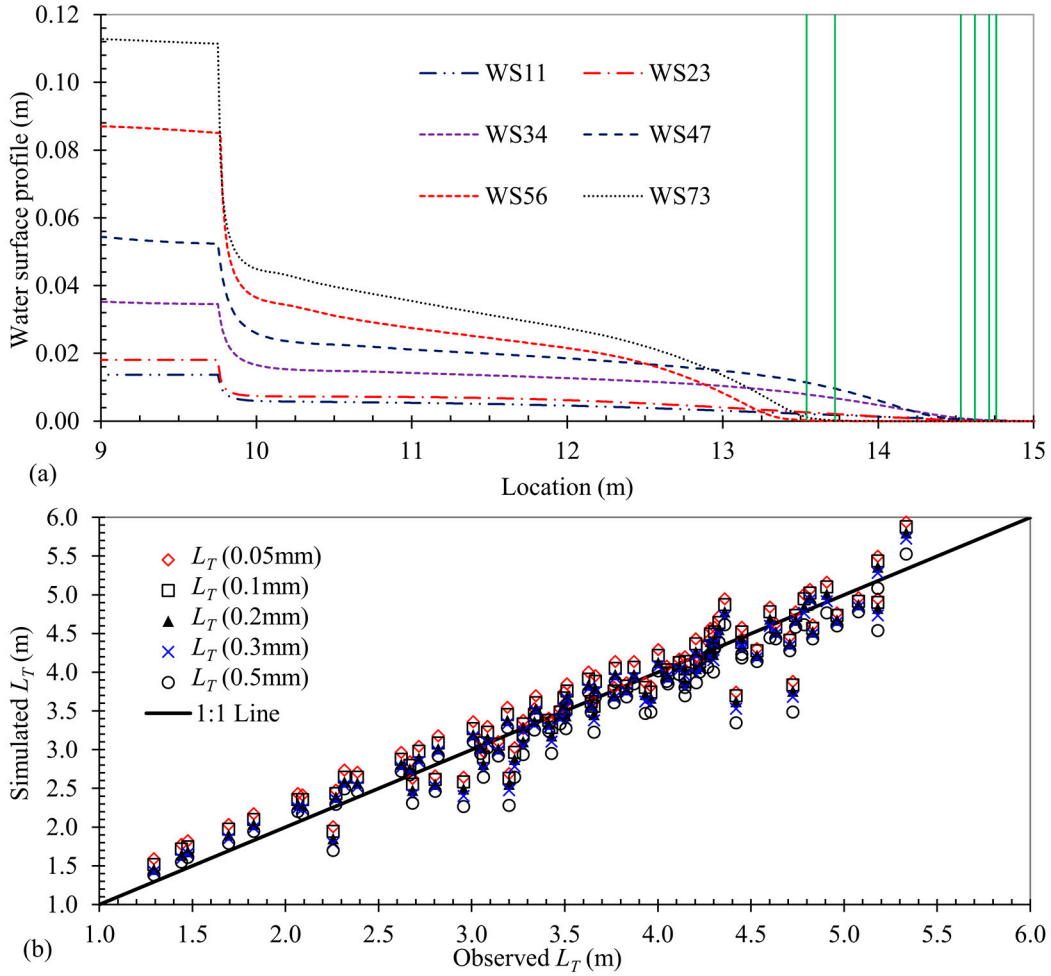

Figure 2. (**a**) Water surface profile along the curb inlet for six selected Wesley's tests (WS11–WS73) and (**b**) comparison of simulated using five depth thresholds (0.05–0.5 mm) and observed 100% interception curb inlet lengths for 80 laboratory tests by Wesley (1961). The solid vertical lines in (**a**) show the location of the water depth equal to the depth limit of 0.2 mm for these six example cases.

Five depth limits (0.05 mm, 0.1 mm, 0.2 mm, 0.3 mm, and 0.5 mm) were tested to determine the end point of the 100% interception curb inlet length. The location of water depth, equal to the depth limit minus the curb inlet start location, was regarded as the 100% interception curb inlet length. The green solid vertical lines in Figure 2a show the location of the water depth equal to the depth limit of 0.2 mm for these six example cases. The simulated curb inlet lengths of total interception for all 80 modeling cases of Wesley's tests were determined using the five water depth limits and compared to L_T observed and determined in laboratory tests (Figure 2b). The final water depth limit was chosen when the root-mean-square error (RMSE) and mean absolute percentage error (MAPE) of simulated and observed curb inlet lengths of total interception were the smallest. Simulated L_T values for the 80 cases/tests ranged from 1.30 m (4.3 ft) to 5.33 m (17.5 ft).

Figure 2b shows that the simulated L_T best matched with observed data when the depth limit for determining L_T was 0.2 mm. The RMSEs for the simulated L_T results with depth limits equal to 0.05, 0.1, 0.2, 0.3, 0.5 mm were 0.30 m, 0.28 m, 0.27 m, 0.29 m, 0.31 m, and 0.34 m, respectively. The corresponding MAPEs for the five depth limits are 7.32%, 6.46%, 6.04%, 6.08%, 6.34%, and 6.80%, respectively. Since the smallest RMSE and MAPE were for the depth limit of 0.2 mm, therefore, the water depth limit 0.2 mm was used for the one thousand modeling cases (O1X1Q1–O10X10Q10) to determine the 100% interception curb inlet lengths summarized in Section 3.3.

Figure 3 shows the comparison of the observed 100% interception curb inlet lengths simulated by the FullSWOF-ZG model and calculated L_T results by three existing methods for the 80 Wesley's lab tests. The RMSE values between observed and calculated L_T from HEC-22 (2009), Izzard (1950), and Muhammad (2018) are 0.56 m, 1.77 m, and 0.45 m, respectively. The corresponding MAPE values are 12.9%, 43.3%, and 7.9%, respectively. The sequence from the smallest to largest RMSE and MAPE values for simulated and calculated L_T results are Simulated < Muhammad < HEC-22 < Izzard. Izzard's equation generally overestimates L_T for all validation cases.

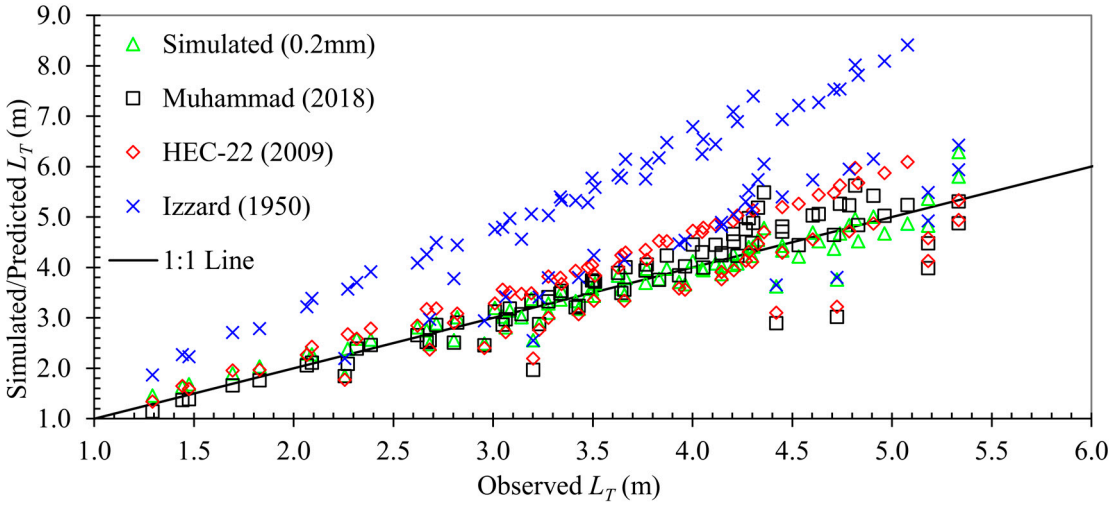

Figure 3. Comparison of simulated/predicted and observed 100% interception curb inlet length L_T for 80 laboratory tests by Wesley (1961).

3.3. Simulated Curb Inlet Lengths of 100% Interception

After L_T was determined for the 1000 modeling cases using FullSWOF-ZG, a generalized power relation, Equation (7) was chosen to develop the regression equation for L_T as a function of four input parameters (Q_{in}, S_0, n, and S_x). Table 1 also shows L_T determined for 10 example cases (OmXmQm, m = 1, 2, . . . , 10) using FullSWOF-ZG. In Equation (7) the Manning's value n and cross slope S_x were grouped as one combined variable, the same as the HEC-22 Equation (3).

$$L_T = kQ_{in}^a S_0^b / (nS_x)^c \quad (7)$$

where L_T is the curb inlet length in m for 100% interception; S_x and S_0 are the cross slope and longitudinal slopes of the road/street (Table 1), Q_{in} is the upstream inflow rate from the road/street surface to the curb inlet in m^3/s (0.006–0.024, Table 1), and n (-) is Manning's roughness of the road surface.

The variation inflation factors (VIF) among three input variables (Q_{in}, S_0, and nS_x) were calculated with MATLAB before developing the equation. The VIFs among the three variables are all equal to 1. This means the predictors are more related to the target variable L_T than they are to each other [32], and the multicollinearity of three variables are not significant. The coefficient k and exponents (a, b, and c) were estimated using the multiple linear regression (MLR) method after the log transformation of Equation (7), and the resulting regression equation of L_T was:

$$L_T = 0.387 Q_{in}^{0.372} S_0^{0.1} / (nS_x)^{0.564} \quad (8)$$

The 95% confidence intervals for the coefficient k and exponents a, b, and c are [0.372, 0.404], [0.368, 0.376], [0.0977, 0.103], and [0.559, 0.568] with p-value < 0.0001, respectively. If L_T is in feet and Q_{in} is in ft^3/s for English or US customary units, the coefficient k would be 0.337. Comparing Equation (8) with HEC-22's L_T Equation (3), the exponent of S_0 in Equation (8) is 0.1 (1/3 of 0.3 in Equation (3)), and the coefficient is about a half. Muhammad's L_T Equation (5) made the coefficient to be much smaller (~1/8 of 0.817 in HEC-22), but other exponents are similar, in addition to having different exponents for n and S_x.

Figure 4a shows the comparison of fitted L_T calculated using Equation (8), and simulated L_T. The R^2 and RMSE between fitted and simulated L_T are 0.99 (Figure 4a) and 0.13 m, respectively. The MAPE between fitted and simulated L_T is 2.34% for all 1000 cases. It shows the fitted L_T or predicted by the regression equation matched well with the simulated L_T when L_T < 5 m, while the difference between simulated and predicted L_T becomes larger when L_T > 5 m. The ratio (R_{lt}) of fitted L_T calculated using Equation (8) and simulated L_T was computed for all 1000 modeling cases; then, the mean R_{lt} and standard deviation for each 100 cases with the same S_0 were also calculated and plotted in Figure 5. The ratio R_{lt} ranged from 0.89 to 1.06 (maximum of 11% underestimate and 6% overestimate), and the 915 fitted L_T values were within 5% from simulated L_T ($0.95 < R_{lt} \leq 1.05$) for Equation (8).

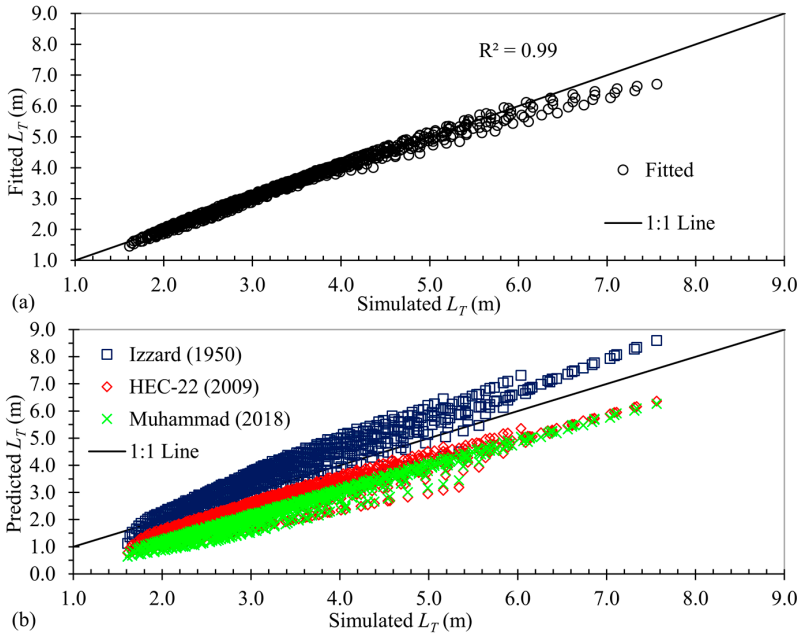

Figure 4. (**a**) Comparison of fitted and simulated 100% interception curb inlet lengths, L_T with Equation (8), and (**b**) predicted from Izzard (1950), HEC-22 (2009), and Muhammad (2018) versus simulated L_T for 1000 modeling cases.

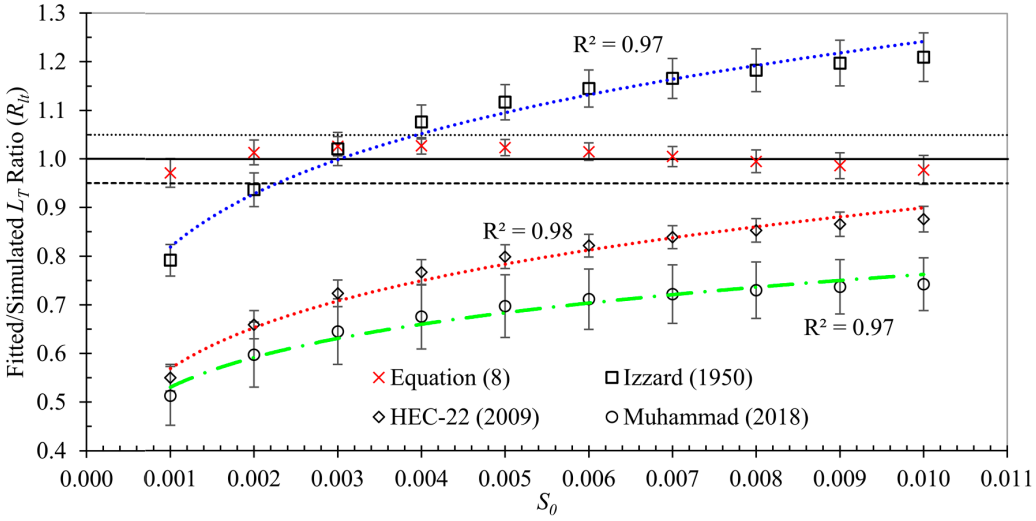

Figure 5. The mean ratio R_{lt} of fitted/predicted and simulated L_T as a function of longitudinal slope S_0 for 1000 modeling cases with standard deviations.

Figure 4b shows a comparison of predicted L_T results with Izzard (1950), HEC-22 (2009), and Muhammad (2018) methods to the simulated results, and the corresponding predicted L_T in m has ranges of [1.12, 8.60], [0.78, 6.36], and [0.63, 6.27], respectively. The predicted L_T for all three methods had strongly linear correlations with simulated L_T with R^2 of 0.91–0.97. The MAPEs between predicted from HEC-22 (2009), Izzard (1950), and Muhammad (2018) and simulated L_T for all 1000 cases were 22.4%, 14.0%, and 32.3%, respectively; the corresponding RMSEs were 0.13 m, 0.22 m, and 1.01 m. The HEC-22 and Muhammad methods underestimate L_T with R_{lt} ranging from 0.48 to 0.92 (0.78 ± 0.10 for average and standard deviation) and from 0.39 to 0.84 (0.68 ± 0.09), respectively. The R_{lt} range for Izzard method was [0.70, 1.28] with an average and standard deviation of 1.08 and 0.13. For the Izzard method, 771 cases overestimated the simulated L_T.

Figure 5 shows the average plus/minus the standard deviation of R_{lt} for Equation (8), Izzard (1950), HEC-22 (2009), and Muhammad (2018) with respect to different S_0 values. All mean R_{lt} ratios were within the range [0.95, 1.05] with small standard deviations (0.02–0.03) for fitted Equation (8), which indicate that the Equation (8) matches very well with simulated L_T for all S_0 conditions. For HEC-22 and Muhammad methods, $R_{lt} < 0.95$ for all S_0 situations and the Muhammad method has a larger standard deviation (0.05–0.07), which means the HEC-22 and Muhammad methods underestimate L_T in a greater extent under smaller S_0 situations. For the Izzard method, most of $R_{lt} > 1$ (overestimates L_T) when $S_0 \geq 0.3\%$, and it underestimates L_T when $S_0 < 0.3\%$. For three previous methods, the mean R_{lt} strongly correlates with S_0 as a power function with $R^2 > 0.97$ (Figure 5): R_{lt} increases with the increase of S_0.

3.4. 100% Intercepted Gutter Flow for Drainage and Road Bioretention Design

The simulated L_T ranged from 1.61 to 7.56 m for the 1000 modeling cases (Figure 4a). In urban drainage design, the inlet opening lengths for various types of curb inlets standardized by municipalities and transportation agencies have only a few preset/pre-cast/manufactured lengths; for example, Texas Type C and Type D curb inlets [7] and TxDOT precast curb inlet outside roadway (PCO) on-grade curb inlets [31] have three opening lengths of 1.52 m (5 ft), 3.05 m (10 ft), and 4.57 m (15 ft). When the calculated curb inlet length for 100% interception is large under design gutter flow, none of the very large opening curb inlets are actually used, but continuously depressed gutter or locally depressed inlets with necessary transient lengths are typically designed and built. Therefore, Equation (8) from the current study, Equation (1) from Izzard (1950), Equation (3) from HEC-22 (2009), and Equation (5) from Muhammad (2018) were rearranged to determine the gutter flow for 100% interception (Q_{g100}) when the curb inlet length is given.

$$Q_{g100} = 12.832(nS_x)^{1.516} L_{ci}^{2.688} / S_0^{0.269} \quad (9)$$

$$Q_{g100-Izzard} = 0.410(nS_x)^{9/7} L_{ci}^{16/7} / S_0^{9/14} \quad (10)$$

$$Q_{g100-HEC-22} = 1.618(nS_x)^{1.429} L_{ci}^{2.381} / S_0^{0.714} \quad (11)$$

$$Q_{g100-Muhammad} = 131.360 n^{2.021} S_x^{1.596} L_{ci}^{2.128} / S_0^{0.553} \quad (12)$$

All the above equations are for the International System of Units (SI) where L_{ci} is in m and Q_{g100} is m^3/s. Determining Q_{g100} helps us to reevaluate these L_T equations. For urban drainage design, design discharge for the gutter was calculated first based on the catchment area, runoff coefficients of land use, and design rainfall intensity; then, the distance between two curb inlets and the curb inlet opening were calculated and selected/specified for the design.

Figure 6 shows the comparison of predicted Q_{g100} from Equations (10)–(12) and from Equation (9) for undepressed curb inlets with L_{ci} = 5 ft (1.524 m). Fourteen S_0 values were used for Figure 6 and from 0.003 (0.3%) to 0.04 (4%), and two small S_0 (0.001 and 0.002) in Table 1 were not used (HEC-22 recommends S_0 > 0.3%), and six larger S_0 (0.015, 0.03, 0.025, 0.03, 0.035, and 0.04) were added to represent the steep-slope roads for urban drainage and road bioretention curb inlet design. The 14 S_0 and 10 S_x (Table 1, 1.5–6%) formed 140 slope combinations that were used to compare/evaluate the above Q_{g100} equations in Figure 6. Even the overall R^2 for linear correlations of Q_{g100} predicted from three previous studies and the newly developed Equation (9) are greater than 0.80, where Q_{g100} predicted by HEC-22 (2009) and Muhammad (2018) is much larger than Q_{g100} predicted by Equation (9). Muhammad's equation has the largest mean absolute percent deviation (MAPD), equal to 180.5%, which always overestimates Q_{g100} (Figure 6), in comparison to Q_{g100} from the current study. The MAPD for Izzard (1950) and HEC-22 (2009) are 25.8% and 69.1%, respectively.

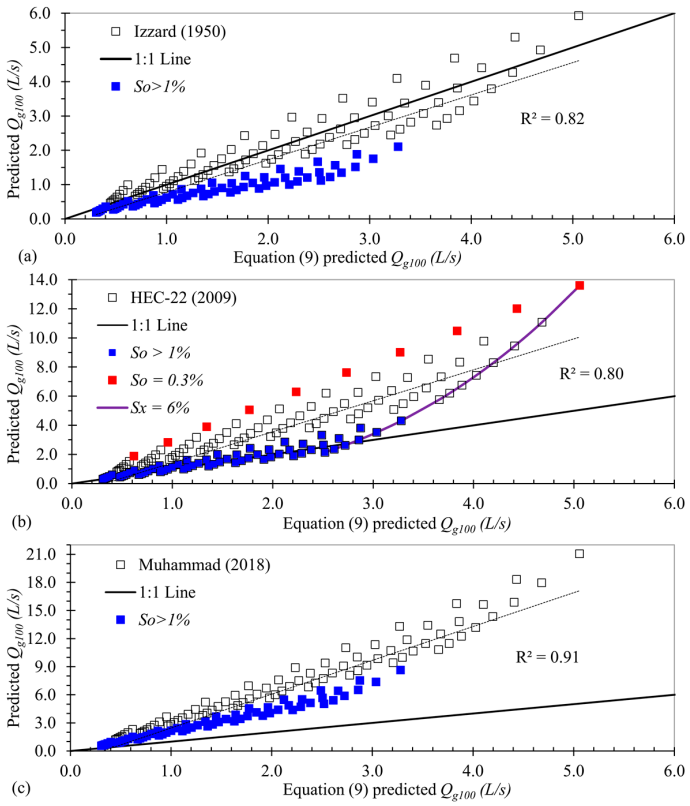

Figure 6. Comparison of predicted 100% interception gutter flow Q_{g100} of L_{ci} = 5 ft (1.524 m) using Equations (10)–(12) from four methods, (**a**) comparison of Izzard (1950) and Equation (9), (**b**) comparison of HEC-22 (2009) and Equation (9), and (**c**) comparison of Muhammad (2018) and Equation (9).

Hodges et al. [31] compared Q_{g100} predicted using HEC-22 equation and their experimental measurements. When S_x was fixed at 6% and S_0 changed from 4% to 0.1%, the Q_{g100} predicted using the HEC-22 equation increased about 6 times, but experimental measurements only increased less than 1.6 times. The purple line on Figure 6b shows the comparison of HEC-22 and Equation (9) predicted Q_{g100} results when S_x = 0.06 (6%). When S_0 decreased from 4% to 0.3% at S_x = 6%, Q_{g100} calculated using HEC-22 increased 6.4 times but Q_{g100} from Equation (9) only increased two times, which is similar to results from the physical model by Hodges et al. [31]. The smaller exponent 0.269 for S_0 in Equation (9) for the current study seems to give a better prediction on Q_{g100} compared to HEC-22 Equation (11).

In Figure 6b, 10 red filled squares gave Q_{g100} predicted from HEC-22 for S_0 = 0.3%, and S_x increased from 1.5% to 6%, and Q_{g100} increased from 1.8 L/s to 13.6 L/s that was, on average, 2.83 times larger than Q_{g100} (0.62–5.1 L/s) from Equation (9). At S_0 = 0.3%, the ratio of Q_{g100} predicted from HEC-22 to Equation (9) ranged from 2.69 to 3.03 with a standard deviation from the mean of 0.11, which graphically shows as a perfect linear relation of these red filled squares on Figure 6b. This strong linear correlation of Q_{g100} predicted from three previous studies versus Equation (9) exists for all other S_0 when S_x is changed. The ratio of Q_{g100} predicted from HEC-22 (2009) versus Equation (9) ranges from 0.85 to 3.03, and has a strong correlation with the longitudinal slope S_0: a power function $Q_{g100\text{-}HEC\text{-}22}/Q_{g100\text{-}Equation\text{-}9}$ = 0.213 $S_0^{-0.445}$ (R^2 = 0.99). Actually, the power function can be approximately derived by dividing Equation (11) to Equation (9). The power function clearly indicates that over-prediction occurs in smaller S_0 because of the negative exponent −0.445; for example, S_0 = 0.3%, as shown by the red filled squares. The blue filled squares on Figure 6 show results for 60 cases with S_0 > 1% and S_x from 1.5% to 4%. From the power function, when S_0 is larger, the ratio of Q_{g100} is smaller, as is also clearly shown in Figure 6 by the blue filled squares for all three methods. Figure 6b shows that the predicted Q_{g100} from HEC-22 matched very well with the ones predicted from Equation (9) when S_0 > 1%. This means both HEC-22 and the newly developed Equation (9) do a very good job to predict Q_{g100} (or L_T using Equation 8) when S_0 > 1%. HEC-22's Equation (3) for L_T and rearranged Equation (11) for Q_{g100} have exponents for slopes S_0 and S_x that were adjusted from Izzard's Equation (1) using limited available experiments, but HEC-22 did not document clearly what specific experimental data were used, which could be for experiments S_0 > 1%. The over-prediction of HEC-22 on Q_{g100} actually only occurs at lower longitudinal slopes; this could be because the HEC-22 equation was not adjusted with experimental data of small S_0. The ratio of Q_{g100} predicted from HEC-22 (2009) versus Equation (9) also seems to correlate with the ratio S_x/S_0 and becomes larger (over-prediction) when the ratio S_x/S_0 increases. The power function of the Q_{g100} ratio versus the ratio S_x/S_0 has a determination coefficient of 0.69, which is much weaker than the correlation with S_0 only (R^2 = 0.99).

Hodges et al. [31] also show that, when the curb length L_{ci} = 10 ft, S_x was fixed at 6%, and S_0 changed from 4% to 0.1%, Q_{g100} calculated using HEC-22 equation over-predicts by an average factor of 1.51 when compared to measured Q_{g100} from their physical model. The ratio of Q_{g100} predicted from HEC-22 (2009) versus measurements actually ranges from 0.81 to 3.0, and the ratio of Q_{g100} predicted from HEC-22 versus Equation (9) also ranges from 0.85 to 2.37 (Figure 6), and these two results are very similar. The comparison of predicted 100% intercepted gutter flow with Equations (10)–(12) to Equation (9) for curb length L_{ci} = 10 ft (3.048 m) and L_{ci} = 15 ft (4.572 m) also gives similar results discussed above for L_{ci} = 5 ft (1.524 m) cases, and are therefore not repeated here.

3.5. Simulated Curb Inlet Efficiency and Evaluation Equation

Table 1 shows E_{ci} determined for 10 example cases (OmXmLm, m = 1, 2, … , 10), which range from 15.3–75.7%. E_{ci} was calculated as the curb inlet outflow divided by the upstream inflow (Figure 1) when the flow through the curb inlet reaches the equilibrium—in other words, the E_{ci} change is less than 0.0005. For the second set of 1000 modeling cases (O1X1L1 to O10X10L1) of 10 different L_{ci} values (Table 1), the mean and standard deviations of simulated E_{ci} at the same L_{ci} were calculated. The mean E_{ci} increased from 12.8% to 84.2%, and the corresponding standard deviation increased from 5.2% to

11.8% when L_{ci} increased from 0.15 m to 1.50 m. This means inlets in the Philadelphia area (the survey conducted by Stoolmiller et al. [5]) could intercept different amounts of stormwater runoff to road bioretention facilities, and some of them were under-designed and had flooding risks on the road.

The format of Equation (6) was used to develop a new relationship between E_{ci} and L_{ci}/L_T using 1000 simulated E_{ci} for 10 different L_{ci} when Q_{in} was a constant of 10 L/s. Even E_{ci} has a strong correlation with L_{ci} (R^2 = 0.86 for a power function), but L_{ci}/L_T is used in Equation (13) so that it can be applied to other flow rates Q_{in} from upstream road or watershed, since L_T (Equation (8)) links with and has the impact of the input parameters S_0, S_x, Q_{in}, and n.

$$E_{ci} = 1 - [1 - (L_{ci}/L_T)]^{2.42} \quad (13)$$

The exponent α was determined based on the simulated E_{ci} results of 1000 cases with the MLR method. The 95% confidence intervals for the exponents α is [2.408, 2.4358] with p-value < 0.0001. Figure 7a shows how the comparison of fitted and simulated E_{ci}; and fitted E_{ci} matches well with the simulated E_{ci} with R^2 = 0.98. Figure 7b shows E_{ci} versus L_{ci}/L_T from the current study (fitted Equation 13), Izzard (1950), HEC-22 (2009), and Muhammad (2018). Fitted Equation (13) is almost the same as Izzard's Equation (2) since α = 2.5, but the HEC-22 equation gives lower E_{ci}. E_{ci} predicted from Muhammad's equation has a different distribution (Figure 7b): different E_{ci} for the same L_{ci}/L_T when S_x is different, since the exponent α is not a constant but a function of S_x.

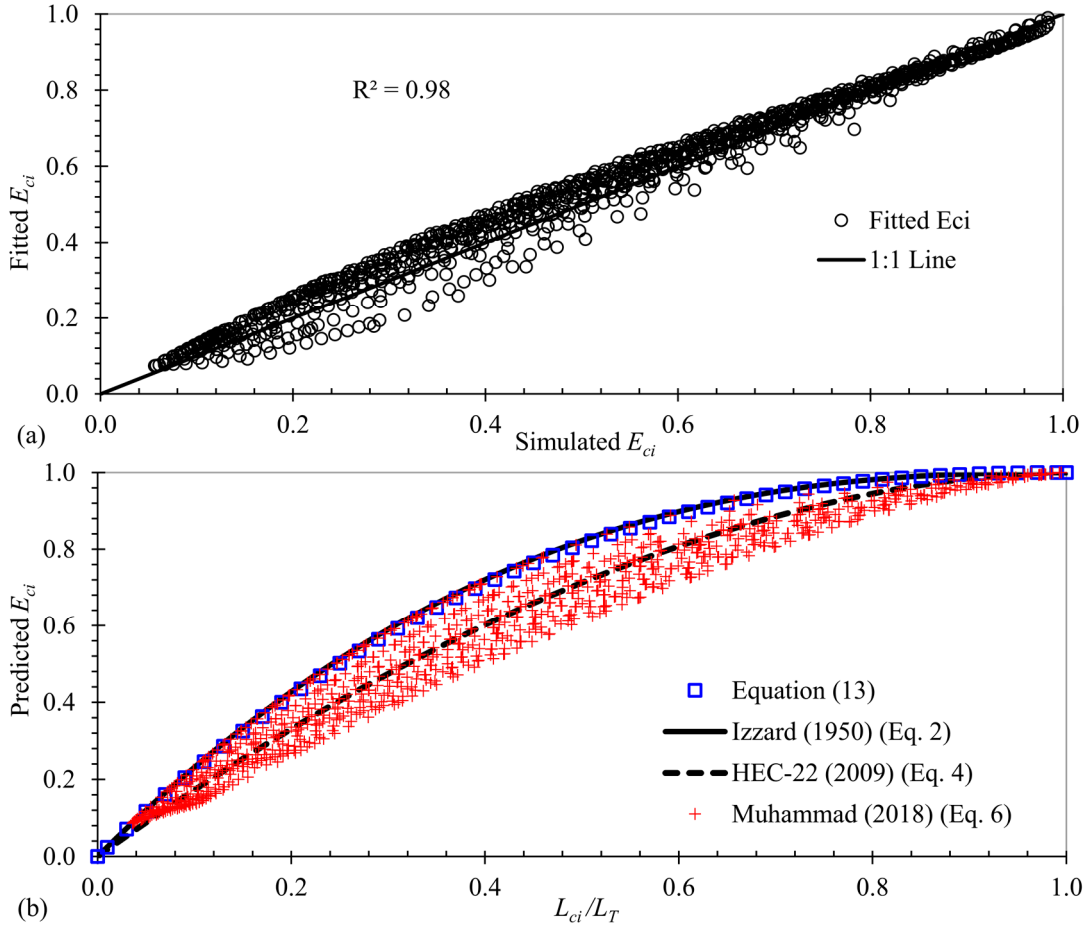

Figure 7. Comparison of fitted or predicted and simulated curb inlet interception efficiency E_{ci}, (**a**) comparison of fitted and simulated E_{ci}, (**b**) relationship between predicted E_{ci} of L_{ci}/L_T.

Figure 8 shows the comparison between predicted E_{ci} from Izzard (1950), HEC-22 (2009), and Muhammad (2018) method and fitted E_{ci} from newly developed Equations (8) and (13) for 10,000 design

cases that are all combinations for 10 S_0, 10 S_x, 10 Q_{in}, and 10 L_{ci} listed in Table 1. The corresponding L_T equation for each method was applied first before L_{ci}/L_T, and then E_{ci} were calculated. When applying E_{ci} equations, E_{ci} was assumed to be 100% when L_{ci} is greater than L_T or $L_{ci}/L_T > 1$. Among all 10,000 cases, there are 21, 228, and 523 cases with $L_{ci}/L_T > 1$ for Izzard, HEC-22, and the Muhammad method when the predicted L_T is smaller than L_{ci}.

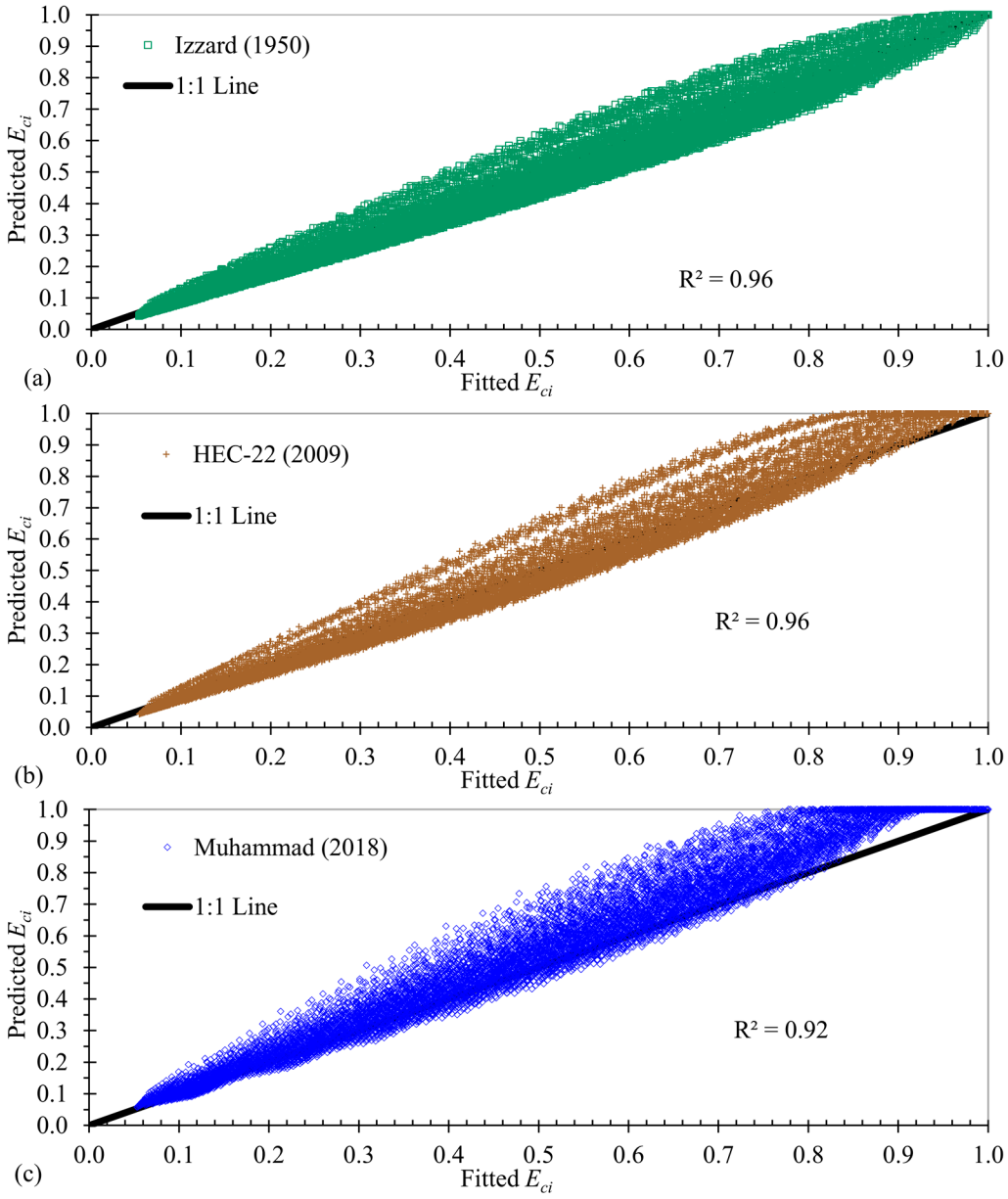

Figure 8. Predicted E_{ci} from Izzard (1950), HEC-22 (2009), and Muhammad (2018) versus fitted E_{ci} for 10,000 design cases for all 10 S_0, S_x, Q_{in}, and L_{ci} combinations in Table 1, (**a**) comparison of Izzard (1950) and fitted results, (**b**) comparison of HEC-22 (2009) and fitted results, (**c**) comparison of Muhammad (2018) and fitted results.

The R^2, RMSE, and MAPD between predicted E_{ci} for Izzard (1950) method and newly developed equations (Equations (8) and (13)) are 0.96, 4.8%, and 8.8%, respectively. The R^2, RMSE, and MAPD of predicted E_{ci} between the HEC-22 (2009) method and newly developed equations are 0.96, 5.9%, and 9.4%, respectively. The R^2, RMSE, and MAPD of predicted E_{ci} between Muhammad's (2018) method and newly developed equations are 0.92, 8.1%, and 12.9%, respectively. This indicates that for the 10,000 undepressed curb inlet cases from all S_0, S_x, Q_{in}, and L_{ci} combinations, when L_T and E_{ci} equations

for each method are applied together to determine the inlet efficiency, the Izzard (1950), HEC-22 (2009), and Muhammad (2018) methods produced similar results, in comparison to E_{ci} from newly developed equations for L_T and E_{ci}. The ratio (R_{ci}) of predicted and fitted E_{ci} was computed and summarized to compare these four methods. For the Izzard (1950) method, the ratio R_{ci} ranged from 0.81 to 1.32 (maximum of 19% underestimate and 32% overestimate in comparison to fitted E_{ci}), and 2921 cases out of 10,000 cases were within 5% from simulated E_{ci} ($0.95 \leq R_{ci} \leq 1.05$). For the HEC-22 (2009) method, the ratio R_{ci} ranged from 0.79 to 1.39 (maximum of 21% underestimate and 39% overestimate), and 3251 cases were within 5% from simulated E_{ci} ($0.95 \leq R_{ci} \leq 1.05$). For the Muhammad (2018) equation, the ratio R_{ci} ranged from 0.80 to 1.74 (maximum of 20% underestimate and 74% overestimate), and 2516 cases were within 5% from simulated E_{ci} ($0.95 \leq R_{ci} \leq 1.05$). There were 3160, 4753, and 8246 cases out of 10,000 cases overestimated E_{ci} ($R_{ci} > 1.0$) for the Izzard (1950), HEC-22 (2009), and Muhammad (2018) methods in comparison to E_{ci} from Equation (13). The HEC-22 underestimated L_T for most of the cases (Figure 4) and then made L_{ci}/L_T larger. There were still 4757 cases overestimating E_{ci} even though the L_{ci}/L_T exponent for HEC-22's E_{ci} Equation (4) was smaller than the exponent in the proposed Equation (13) and Izzard's Equation (2). Figure 8 shows that the Izzard's method and newly developed equations gave the most similar E_{ci} predictions, and that the HEC-22 method gave the next most similar predictions on E_{ci}.

4. Summary and Conclusions

In this study, the updated FullSWOF-ZG program based on the open-source overland flow simulation program FullSWOF_2D was tested with 20 different locally depressed Texas type D curb inlet cases to simulate inlet efficiency. The differences between simulated and observed E_{ci} ranged from −2.28% to 4.21% with the average ± standard deviation being 1.10% ± 1.67%. The FullSWOF-ZG program was also validated using 80 laboratory tests to simulate the curb inlet length of 100% interception with an RMSE equal to 0.27 m and MAPE equal to 6.04%. These validation runs indicated that the FullSWOF-ZG program can accurately simulate the overland flow through the curb inlets with the high agreement and small error with observed ones so that it can be used to determine L_T and E_{ci}. One thousand undepressed curb inlet modeling cases of the road with 10 S_0, 10 S_x, and 10 Q_{in} were established and modeled to determine L_T, and then a new estimation equation of L_T was developed by the regression with the input parameters. The second set of 1000 road modeling cases of undepressed curb inlets with 10 S_0, 10 S_x, and 10 L_{ci} and a constant Q_{in} (10 L/s) were established and modeled to determine E_{ci}, and then a new estimation equation of E_{ci} was developed as a function of L_{ci}/L_T. The newly developed L_T equation was compared with three previous methods, including Izzard (1950), HEC-22 (2009), and Muhammad (2018) for predicting L_T for 1000 undepressed curb inlet cases. Finally, L_T and E_{ci} equations for four methods were applied together to predict E_{ci} for 10,000 curb-inlet cases of all ten S_0, S_x, Q_{in}, and L_{ci} combinations listed in Table 1. Predicted E_{ci} values for all 10,000 cases from Izzard (1950), HEC-22 (2009), and Muhammad (2018) method had RMSE < 8.5% and MAPD < 13% in comparison with ones from the newly developed L_T and E_{ci} equations in this study. The newly developed equations gave more accurate estimations of L_T and E_{ci} over a wide range of input parameters. These equations can be applied to design urban drainage and road bioretention facilities since they were developed using a large number of simulation runs with diverse input parameters, but previous methods often overpredict the gutter flow Q_{g100} of total interception when longitudinal slope S_0 is small. Also, simulation runs were done after the FullSWOF-ZG program for overland flow simulation was comprehensively validated with 100 laboratory tests. In future studies, the equations used to evaluate efficiency of locally depressed and continuously depressed curb inlets can be developed using simulation results from the FullSWOF-ZG program. The hydraulic-performance-based equations for different types of curb inlets should be promoted for the design of road bioretention facilities, instead of only considering landscape and safety perspective.

Author Contributions: X.L. updated the FullSWOF_2D program, conducted the simulations and analysis of the results, prepared the manuscript draft. X.F. supervised the model development, simulation runs, data analysis; and revised the manuscript. G.C., Y.G., J.W. and J.L. provided inputs on the writing, data analysis, and revised the manuscript. All authors made contributions to the study and writing the manuscript.

Funding: The research was partially supported by the National Natural Science Foundation of China (No. 51478026), Beijing Higher Education High-Level Teachers Team Construction Program (CIT & TCD 201704055), and Beijing University of Civil Engineering and Architecture Research Fund for Pyramid Talents Development.

Acknowledgments: Thanks to Muhammad Ashraf from the University of Texas at Austin organizing and sharing curb inlet laboratory experimental data for previous studies. The author, X.L., wishes to express his gratitude to the Chinese Scholarship Council for financial support pursuing his graduate study at Auburn University.

Conflicts of Interest: The authors declare no conflict of interest.

References

1. Starzec, M.; Dziopak, J.; Słyś, D.; Pochwat, K.; Kordana, S. Dimensioning of Required Volumes of Interconnected Detention Tanks Taking into Account the Direction and Speed of Rain Movement. *Water* **2018**, *10*, 1826. [CrossRef]
2. Li, X.; Li, J.; Fang, X.; Gong, Y.; Wang, W. Case studies of the sponge city program in China. In Proceedings of the World Environmental and Water Resources Congress, West Palm Beach, FL, USA, 22–26 May 2016; American Society of Civil Engineers: Reston, VA, USA, 2016; pp. 295–308.
3. Li, X.; Fang, X.; Gong, Y.; Li, J.; Wang, J.; Chen, G.; Li, M.-H. Evaluating the road-bioretention strip system from a hydraulic perspective—Case studies. *Water* **2018**, *10*, 1778. [CrossRef]
4. Tu, M.-C.; Traver, R. Clogging impacts on distribution pipe delivery of street runoff to an infiltration bed. *Water* **2018**, *10*, 1045. [CrossRef]
5. Stoolmiller, S.; Ebrahimian, A.; Wadzuk, B.M.; White, S. Improving the design of curb openings in green stormwater infrastructure. In Proceedings of the International Low Impact Development Conference, Nashville, TN, USA, 12–15 August 2018; Environmental & Water Resources Institute: Nashville, TN, USA, 2018; pp. 168–176.
6. Liang, X. Hydraulic calculation and design optimization of curb opening in Sponge City construction. *China Water Wastewater* **2018**, *34*, 42–45. (In Chinese)
7. Hammonds, M.A.; Holley, E. *Hydraulic Characteristics of flush Depressed Curb Inlets and Bridge Deck Drains*; FHWA-TX 96-1409-1; Texas Department of Transportation: Austin, TX, USA, 1995.
8. Izzard, C.F. Tentative results on capacity of curb opening inlets. In Proceedings of the 29th Annual Conference of the Highway Research Board, Washington, DC, USA, 13–16 December 1949; Highway Research Board: Washington, DC, USA, 1950; pp. 11–13.
9. Li, W.H. Hydraulic theory for design of stormwater inlets. In Proceedings of the 33rd Annual Meeting of the Highway Research Board, Washington, DC, USA, 12–15 January 1954; Highway Research Board: Washington, DC, USA, 1954; pp. 83–91.
10. Brown, S.; Stein, S.; Warner, J. *Urban Drainage Design Manual: Hydraulic Engineering Circular No. 22 (HEC-22)*; FHWA-NHI-10-009 HEC-22; National Highway Institute: Arlington, VA, USA, 2009.
11. Jens, S. *Design of Urban Highway Drainage*; FHWA-NHI-10-009 HEC-22; Federal Highway Administration: Washington, DC, USA, 1979; pp. 198–226.
12. Johnson, F.L.; Chang, F.F. *Drainage of Highway Pavements: Hydraulic Engineering Circular No. 12 (HEC-12)*; FHWA-TS-84-202 HEC No.12; Federal Highway Administration: McLean, VA, USA, 1984; pp. 39–64.
13. Muhammad, M.A. *Interception Capacity of Curb Opening Inlets*; University of Texas at Austin: Austin, TX, USA, 2018.
14. Guo, J.C.Y.; MacKenzie, K. *Hydraulic Efficiency of Grate and Curb-Opening Inlets Under Clogging Effect (CDOT-2012-3)*; Colorado Department of Transportation, DTD Applied Research and Innovation Branch: Denver, CO, USA, 2012.
15. Uyumaz, A. Urban drainage with curb-opening inlets. In Proceedings of the Ninth International Conference on Urban Drainage (9ICUD), Portland, OR, USA, 8–13 September 2002; American Society of Civil Engineers: Portland, OR, USA, 2002; pp. 1–9.
16. Schalla, F.E.; Ashraf, M.; Barrett, M.E.; Hodges, B.R. Limitations of traditional capacity equations for long curb inlets. *Transp. Res. Rec.* **2017**, *2638*, 97–103. [CrossRef]

17. Comport, B.C.; Thornton, C.I. Hydraulic efficiency of grate and curb inlets for urban storm drainage. *J. Hydraul. Eng.* **2012**, *138*, 878–884. [CrossRef]
18. Russo, B.; Gómez, M. Discussion of "hydraulic efficiency of grate and curb inlets for urban storm drainage" by Brendan C. Comport and Christopher I. Thornton. *J. Hydraul. Eng.* **2013**, *140*, 121–122. [CrossRef]
19. Wasley, R.J. Hydrodynamics of flow into curb-opening inlets. *J. Eng. Mech. Div.* **1961**, *87*, 1–18.
20. Delestre, O.; Darboux, F.; James, F.; Lucas, C.; Laguerre, C.; Cordier, S. FullSWOF: A free software package for the simulation of shallow water flows. *arXiv* **2014**, arXiv:1401.4125.
21. Fang, X.; Jiang, S.; Alam, S.R. Numerical simulations of efficiency of curb-opening inlets. *J. Hydraul. Eng.* **2009**, *136*, 62–66. [CrossRef]
22. Barréde Saint-Venant, A.J.C. Théorie du mouvement non permanent des eaux, avec application aux crues des rivières et à l'introduction des marées dans leurs lits. *Comptes Rendus des Séances de l'Académie des Sciences* **1871**, *73*, 237–240.
23. Unterweger, K.; Wittmann, R.; Neumann, P.; Weinzierl, T.; Bungartz, H.-J. Integration of FullSWOF_2D and PeanoClaw: Adaptivity and local time-stepping for complex overland flows. In *Recent Trends in Computational Engineering-CE2014*; Springer: Berlin, Germany, 2015; pp. 181–195.
24. Gourbesville, P.; Cunge, J.; Caignaert, G. *Advances in Hydroinformatics-SIMHYDRO 2014*, 1st ed.; Springer: Singapore, 2014; p. 624.
25. Zhang, W.; Cundy, T.W. Modeling of two-dimensional overland flow. *Water Resour. Res.* **1989**, *25*, 2019–2035. [CrossRef]
26. Audusse, E.; Bouchut, F.; Bristeau, M.-O.; Klein, R.; Perthame, B.T. A fast and stable well-balanced scheme with hydrostatic reconstruction for shallow water flows. *SIAM J. Sci. Comput.* **2004**, *25*, 2050–2065. [CrossRef]
27. Cordier, S.; Coullon, H.; Delestre, O.; Laguerre, C.; Le, M.H.; Pierre, D.; Sadaka, G. *FullSWOF Paral: Comparison of Two Parallelization Strategies (MPI and SKELGIS) on a Software Designed for Hydrology Applications*; ESAIM: Proceedings; EDP Sciences: Julius, France, 2013; pp. 59–79.
28. Leandro, J.; Martins, R. A methodology for linking 2D overland flow models with the sewer network model SWMM 5.1 based on dynamic link libraries. *Water Sci. Technol.* **2016**, *73*, 3017–3026. [CrossRef] [PubMed]
29. Li, X.; Fang, X.; Li, J.; KC, M.; Gong, Y.; Chen, G. Estimating time of concentration for overland flow on pervious surfaces by particle tracking method. *Water* **2018**, *10*, 379. [CrossRef]
30. MathWorks. *Matlab and Statistics Toolbox Release 2017a*; The MathWorks Inc.: Natick, MA, USA, 2017.
31. Hodges, B.R.; Barrett, M.E.; Ashraf, M.; Schalla, F.E. *Interception Capacity of Conventional Depressed Curb Inlets and Inlets with Channel Extension*; Texas Department of Transportation: Austin, TX, USA, 2018; pp. 54–57.
32. Chatterjee, S.; Simonoff, J.S. *Handbook of Regression Analysis*; John Wiley & Sons: Hoboken, NJ, USA, 2013; Volume 5.